

<Supplementary Information>

First-principle and experimental investigation of the morphology of layer-structured LiNiO_2 and LiCoO_2

Yongseon Kim,^{1,2} Hyundeok Lee,^{2,3} and Shinhoo Kang^{1,*}

¹Department of Materials Science and Engineering, Seoul National University, Seoul, 151-742, Korea.

²SAMSUNG SDI CO., LTD, Yongin-si, Gyeonggi-do, 446-577, Korea

³Department of Materials Science and Engineering, Korea University, Seoul, 136-713, Korea.

S.1. Synthesis temperature of $\text{LiNi}_{1-x}\text{Co}_x\text{O}_2$

Synthesis condition of cathode materials is different depending on the target property: if small particle size is wanted (generally to get fast rate performance in the application of high power lithium ion batteries), relatively low firing temperature would be desirable, whereas high temperature synthesis is necessary to increase primary particle size and reduce the surface area to control the side reaction at the electrolyte-cathode interface.

Generally commercial LCO is known to be synthesized at near 1000 °C. Optimum firing temperature of Ni-based materials differed with Ni-content. From experiments, we determined optimum firing temperature (the temperature which provided largest charge/discharge capacity) and plotted with respect to Ni-content (Fig. s1). The firing temperature of Ni-based materials is generally lower than LCO, because so-called cation-mixing (partial disorder of Ni and Li-distribution in the crystal) easily occurs in the crystal as the temperature increases. Thus, Ni-based cathode materials are synthesized at lower temperature than LCO in general for the best electrochemical performance, and this may cause difference of particle morphology. However, as discussed in the manuscript, primary crystals of Ni-based materials were still smaller even when their firing condition was same with that of LCO in our experiments.

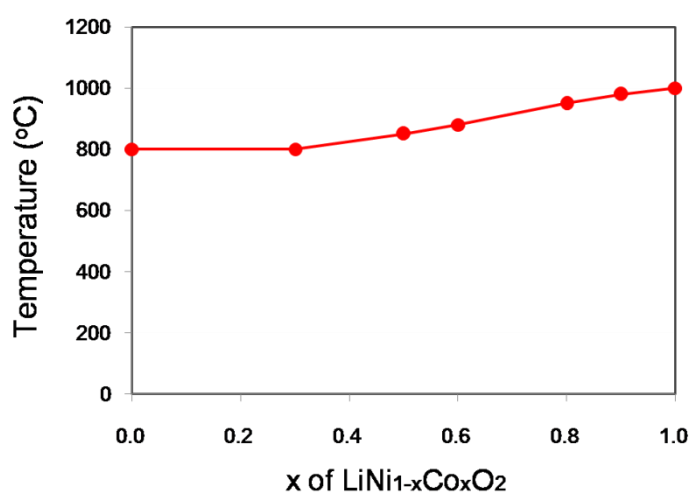


Fig. s1. Optimum firing temperature of lithium nickel cobalt oxides.

S.2. Density of LCO and Ni-based cathode materials

Although LNO has the same crystal structure as LCO, theoretical density (crystal density) of LNO is lower than LCO because lattice parameters of LNO are larger than LCO and atomic weight of Ni is lighter than Co. Thus, as Co-content increases in $\text{LiCo}_x\text{Ni}_{1-x}\text{O}_2$, the crystal density increases. The crystal structure information for $\text{LiNi}_{1-x}\text{Co}_x\text{O}_2$ is rounded up, and crystal density is calculated on the basis. The result is presented Fig. s2.

The tap density and electrode density (electrode density is measured after roll-pressing of the cathode which is composed of cathode powder, carbon, and polymer binder coated on a Al current-collector) of commercial LCO and NCA ($\text{LiNi}_{0.82}\text{Co}_{0.15}\text{Al}_{0.03}$) are presented in Table s2 along with the particle size distribution. Difference of crystal density between LCO and NCA is ~5% (Fig. s2), but the gap of tap density and electrode density is larger, even for similar particle size distribution (see data of LCO and NCA-2 in Table s2). This may indicate that difference of bulk density caused by morphological character of the particles is one of the main factors determining tap- and electrode density.

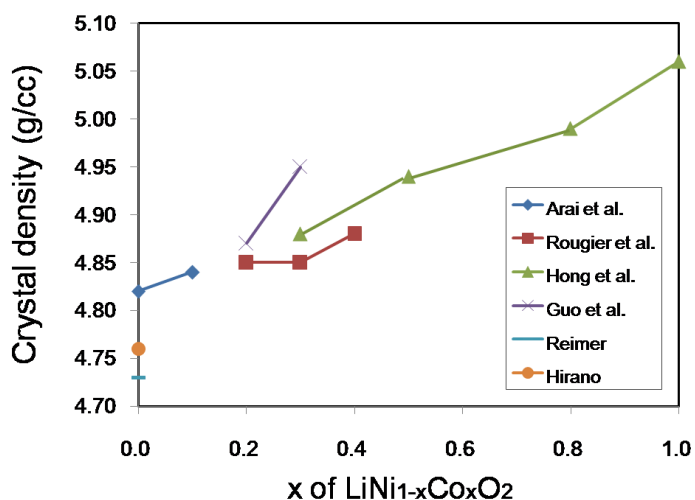


Fig. s2. Crystal density of lithium nickel cobalt oxides.

	Size distribution (μm)			Tap density (g/cc)	Electrode density (g/cc)
	d_{10}	d_{50}	d_{90}		
LCO	4.2	15.3	28.2	2.68	3.93
NCA-1	7.5	12.3	19.6	2.19	3.32
NCA-2	6.6	14.9	25.5	2.23	3.38

Table s2. Particle size distribution, tap density, and electrode density of commercial LCO and NCA.

S.3. SEM images of LCO and LNO

The facet planes discussed in relation with Fig. 2 of the manuscript appeared more clearly with synthesis at higher temperatures. The SEM images of the materials fired at high temperatures are presented in Fig. s3-1. Severe agglomeration occurring with high temperature synthesis required pulverization of the sintered body, and this is why fracture surfaces and broken pieces are observed from the pictures. Particles grown with liquid fluxes such as KCl or NaCl showed more clear facets (Fig. s3-2). And image of particles with clear facet planes are available from References No. 19, 20, and 24.

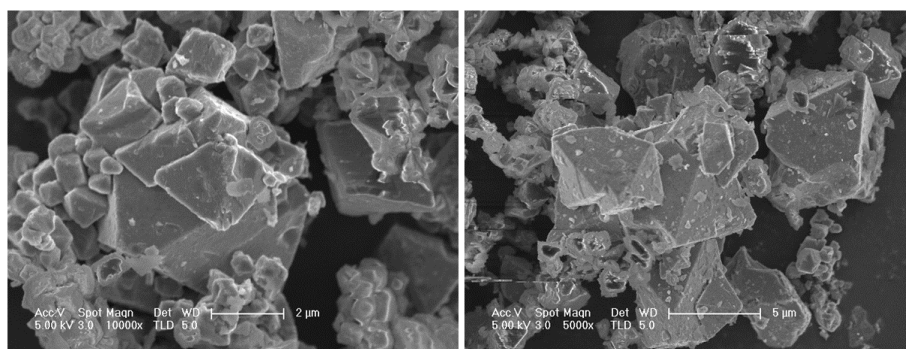


Fig. s3-1. SEM images of LNO fired at 950 °C

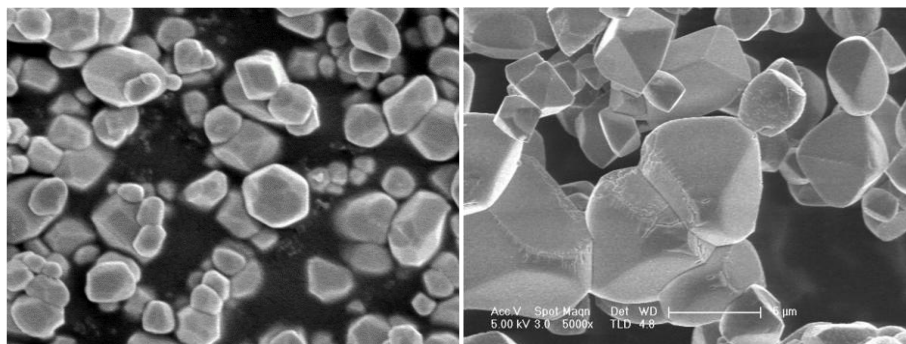


Fig. s3-2. SEM images of LCO and LNO synthesized using alkali fluoride flux

S.4. SEM image of raw materials, XRD pattern of raw materials and synthesized samples

Transition metal hydroxides were used as the starting raw materials after ball-milling in order to make LCO and LNO with the same processing condition and remove difference of morphology caused by the character of the raw materials. The particles were crushed to submicron size, thus it does not seem that morphological character of raw materials has affected particle shape of LCO and LNO (Fig. s4-1). XRD pattern of the hydroxides after ball-milling is presented in Fig. s4-2. The peaks exactly matched with those of $\text{Co}(\text{OH})_2$ and $\text{Ni}(\text{OH})_2$ respectively, though the diffraction peaks are somewhat broad because the crystal was damaged during the milling process. XRD patterns of synthesized samples are shown in Fig. s4-3, which shows LCO and LNO phases are synthesized at the temperatures experimented except a little impurity phases of raw materials for LCO fired at 800 °C.

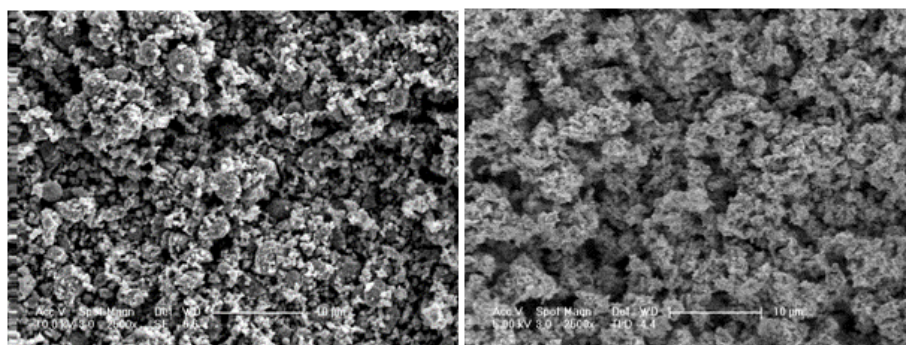


Fig. s4-1. SEM image of $\text{Co}(\text{OH})_2$ and $\text{Ni}(\text{OH})_2$ raw materials. (scale bars: 10 μm)

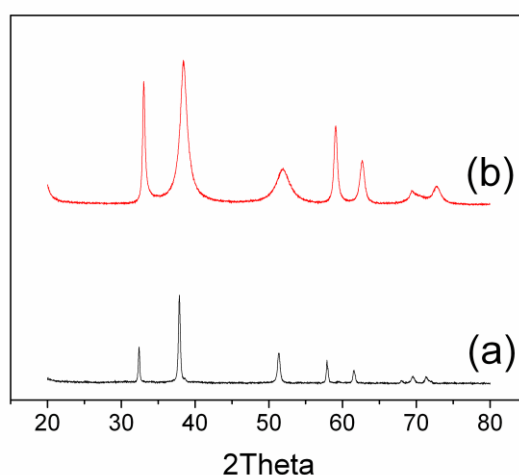


Fig. 4s-2. XRD patterns of transition metal hydroxides after ball-milling:

(a) $\text{Co}(\text{OH})_2$ and (b) $\text{Ni}(\text{OH})_2$.

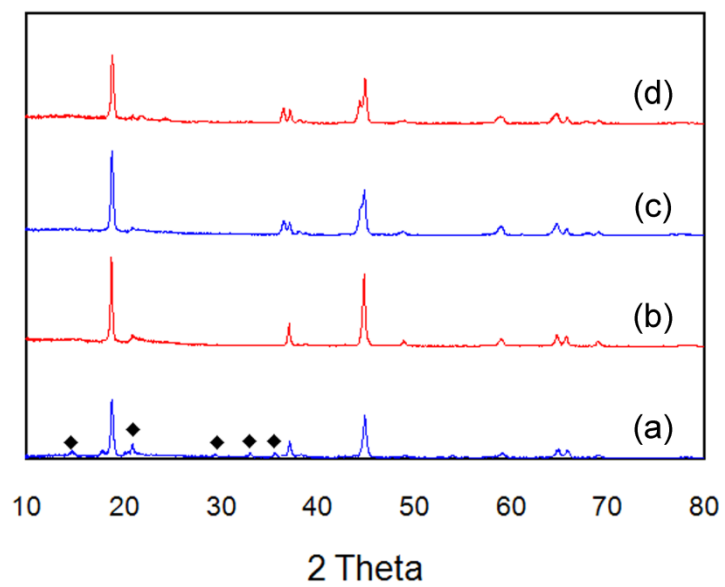


Fig. 4s-3. XRD patterns of synthesized samples:

(a) LCO synthesized at 800 °C, (b) LCO at 900 °C, (c) LNO at 800 °C, and (d) LNO at 900 °C.

S.5. Size distribution of primary particles of the samples whose SEM images are presented in Figure 13 and 14.

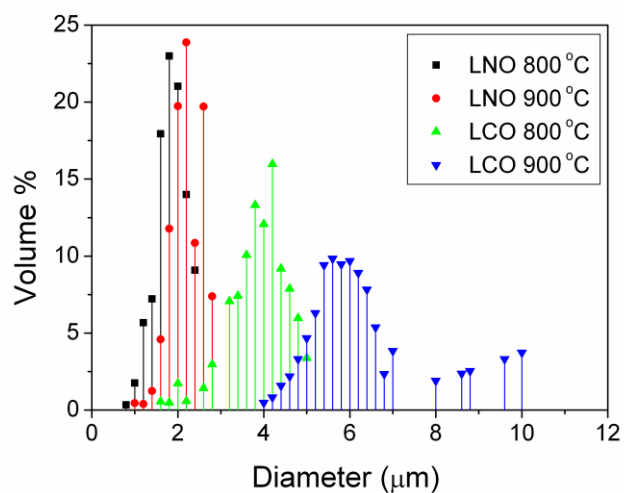


Fig. 5s-1. Size distribution of primary particles of the samples shown in Figure 13 of the manuscript

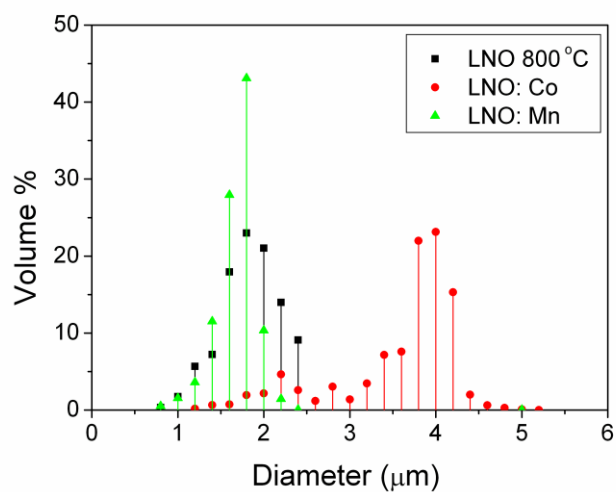


Fig. 5s-2. Size distribution of primary particles of the samples shown in Figure 14 of the manuscript